A.Ahmadvand *et al.* [6] in 2017 has dealt with an interactive natural color images segmentation method. This technique obtains the characteristic of images by means of the nonlinear compact structure tensor (NCST), and subsequently, it utilizes Grab-Cut technique to acquire the segmentation. This process not only recognizes the non-parametric fusion of information and texture information but further develops the effectiveness of the computation. Then, the enhanced Grab-Cut algorithm was employed to estimate the foreground target segmentation so as to compute the efficiency and simplicity. After carrying out a massive amount of researches on synthetic natural images and texture images, the results revealed that this technique had improved accurate segmentation effect.

Yafeng Li *et al.* [7] in 2016 introduced an improved mechanism dependent on image segmentation process that unites feature extraction and image segmentation into a combined design. The implemented design comprises of two parts, namely, multi-scale decomposition part and the segmentation part. In the design, the segmentation part was based on the intensities of the image in the regions of interest whereas the part of multi-scale decomposition was based on the different scale features. The multi-scale decomposition assists the development of segmentation as the region of interest can be identified from a suitable scale easily. The total variation projection regularization (TVPR) was employed to maintain the geometric form of the segmented regions. Based on the geometric importance of TVPR parameters, a selection method for adaptive TVPR parameters was implemented. Numerical models on real and synthetic images were provided to exhibit the efficiency of the proposed technique.

Bacterial foraging-based edge detection (BFED) technique was recommended by Yongsheng Pan *et al.* [8] in 2017 for segmentation of cell images. The rise of intensities as the nutrient attention and propel bacteria to forage beside nutrient-rich locations that imitate the characteristics of Escherichia coli were designed. The nature-inspired evolutionary technique can recognize the required edges and plot them as the bacteria tracks. The outcomes specify that the BFED algorithm recognizes the boundaries more efficiently and offers much better accurate cell image segmentation.

The technique implemented by Weiwei Wang *et al.* [9] in 2017 can be considered as a scheme that interpolates LSR and SSC adaptively based on the correlation between the samples of data. It has the capability for selecting subspaces intended for uncorrelated data in addition to grouping capability for highly correlated data. The outcomes of experiments based on image segmentation demonstrated that the implemented algorithm was more enhanced than the-state-of-art techniques.

In 2014, M. Jogendra kumar *et al.* [1] has introduced various image segmentation methods such as edge based segmentation, thresholding, Neutral Network and region based segmentation and determined the threshold value for it. They have mentioned that the mage segmentation indicates the separation of an image into diverse regions that are similar or homogenous and inhomogeneous in some features like colour, texture or intensity.

Review

The review with features and challenges of diverse conventional segmentation methods are shown in Table 1. The method CWNN exhibits certain unique properties where shift invariance, good directional selectivity, and perfect reconstruction are possible. Limited redundancy and efficient N-order computation are also possible here. There are certain limitations too. The characteristics of SAR image are not considered, and other neural applications are not taken into account in this paper [2]. Wavelet fusion based strategy includes the advantage of improving the segmentation of images, and it allows working in various resolution levels. But there is a lack of real situations that are encountered in the field. It does not offer the chances for changes in the field for representing certain situations that may occur in the future crops [3]. Wavelet-based TCA (WT-TC-MCA) that results in higher precision for different values of recall thus improving texture-based image segmentation. But the method is mostly dependent on texture characteristics and is complex due to the employment of several strategies [4]. Fuzzy GGD based algorithm enhances the grouping of image pixels based on Gaussian density. The merits of this algorithm are not sensitive to initial parameters, but small object segmentation or detection is risky to adopt in block-based reactive elements. Frequency or spatial properties are not incorporated in this strategy, which is said to be a challenge in this paper [5]. Grab-cut algorithm which minimizes or reduces the time for iteration gives more accurate effects of segmented elements. The challenge in this paper is that there is no any supervision of the algorithm and the implemented strategy is still an interactive one [6]. The technique TVPR which possesses the ability to deal with intensity inhomogeneities is also utilized to preserve geometric shapes of the segmented regions. The limitation is that it is complex due to two terms adopted in the TV-L1 model and there are no explanations about the texture component description and bias correction of magnetic resonance images [7]. The Gauss-Newton adaptation strategy which is much suited for parallel processing can also generate one-pixel width, un-fragmented and well-localized edges. Boundary smoothness and cell shape constraints are not explained in this presentation for more accuracy [8]. Correlation adaptive weighted regression (CAWR) mechanism involves the grouping capability for highly correlated data and subspace selection ability for uncorrelated data, but it is somewhat complex due to the adoption of SSC and LSR [9].

Table 1: Review of the state-of-arts methods

Author [citation]	Adopted methodology	Features	Challenges
Yiping Duan *et al*. [2]	CWNN	❖ Shift invariance ❖ Good directional selectivity ❖ Perfect reconstruction ❖ Limited redundancy ❖ Efficient N-order computation	❖ Lack of consideration about the characteristics
M. Guijarro *et al*. [3]	Wavelet fusion-based strategy	❖ Improved image segmentation accuracy ❖ Capable to work under different resolution levels.	❖ Lack of consideration of real scenarios
Jianning Chi *et al*. [4]	WT-TC-MCA	❖ Higher precision for most values of recall. ❖ Improved texture-based image segmentation	❖ Highly dependent on texture characteristics ❖ Complex due to several strategies.
Siu Kai Choy *et al*. [5]	Fuzzy GGD.	❖ Insensitive to initial parameters ❖ Enhancement in grouping image pixels. ❖	❖ Small object detection/segmentation is crucial. ❖ Spatial/frequency features are not incorporated.
A.Ahmadvand *et al*. [6]	Grab-Cut algorithm	❖ Iteration time is reduced. ❖ More accurate segmentation effect.	❖ No supervision of algorithm. ❖ Interactive algorithm
Yafeng Li *et al*. [7]	TVPR	❖ Deal with intensity inhomogeneties. ❖ Preserves geometric shapes of the segmented regions.	❖ Highly complex due to two terms in the TV-L1model. ❖ No explanation of texture component description and bias correction of MRI.
Yongsheng Pan *et al*. [8]	Gauss–Newton adaptation strategy	❖ Suited for parallel processing. ❖ Un-fragmented and well-localized edges	❖ Boundary smoothness is not incorporated ❖ No consideration for cell shapes
Weiwei Wang *et al*. [9]	CAWR	❖ Grouping capability for highly correlated data. ❖ Subspace selection ability for uncorrelated data	❖ Complex due to SSC and LSR. ❖ Low contrast

PROPOSED IMAGE SEGMENTATION FRAMEWORK

The entire architecture of the proposed image segmentation method is given in Fig. 1. Initially, an image $I(x,y)$ is subjected to active contour mechanism, where a mask is applied to segment the required image. By means of the mask, the required or necessary region can be segmented separately which is denoted by $A(x,y)$. Then the original image $I(x,y)$ is subjected to graph cut technique, which involves partitioning of the image into two segments. Here, the image $I(x,y)$ is split into two halves. Thus the two obtained partitions are represented as $B(x,y)$ and $C(x,y)$. The two partitions are then compared with active contour image $A(x,y)$, and intersected regions of the two images are noted that are indicated by $D(x,y)$ and $E(x,y)$. Moreover, an optimization using Fuzzy entropy maximization technique is applied by which both the images $D(x,y)$ and $E(x,y)$ are split into low-intensity images $D_1(x,y)$ and $E_1(x,y)$ and high-intensity images $D_2(x,y)$ and $E_2(x,y)$ respectively. Here, the entropy information is maximized by Non-Linear Programming [36]. From the low density and high-density images, the optimal segmented output is taken after comparison.

The pseudo code of the proposed segmentation process is shown in algorithm 1.

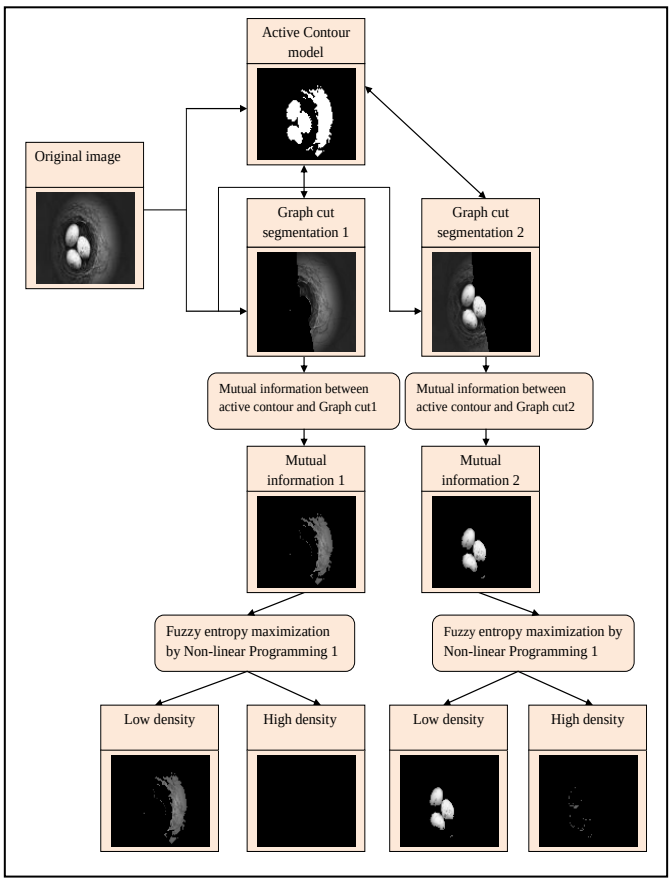

Figure 1: Overall architecture of the proposed AGFES-based image segmentation

Algorithm 1: **Proposed image segmentation model**	
Step 1	Input: Input image $I(x, y)$
Step 2	Output: Segmented image
Step 3	Apply active contour model and attain the segmented output $A(x, y)$
Step 4	Apply graphcut mode and obtain $B(x, y)$ and $C(x, y)$
Step 5	Compare $A(x, y)$ and $B(x, y)$ and take the mutual information as $D(x, y)$
Step 6	Compare $A(x, y)$ and $C(x, y)$ and take the mutual information as $E(x, y)$
Step 7	Apply FEM to $D(x, y)$ and split it into low density and high density images, $D_1(x, y)$ and $D_2(x, y)$
Step 8	Apply FEM to $E(x, y)$ and split it into low density and high density images, $E_1(x, y)$ and $E_2(x, y)$
Step 9	Select the segmented output from four images $D_1(x, y)$, $D_2(x, y)$, $E_1(x, y)$ and $E_2(x, y)$

STAGES OF IMAGE SEGMENTATION

Active contour model

An active contour [28] is an energy reducing spline that identifies particular characteristics within an image. It is a flexible surface or curve that can be dynamically suited to necessary objects or edges in the image. It comprises of a group of control points linked by straight lines. The active contour is referred by the amount of sequence and control points of one another. Setting the active contours to shapes in images is an interactive procedure. The user should recommend a primary contour that is somewhat close to the proposed shape. The contour will subsequently get attracted to the image features extracted by energy that is available internally by generating an attractor image.

It further involves two types of deformable designs, namely, parametric and geometric models. The parametric models comprise surfaces and curves explicitly in parametric form. It involves the formulation for reducing the energy, where the entire energy reduction occurs when external and internal energies are similar. Further dynamic force is formulated which facilitates the employment of general external forces. Geometric deformable models are dependent on the level set technique and the theory of curve evolution. It further leads to the independent evolution from parametric form. The surfaces or curves produced depend on the multidimensional functions level sets. By adopting this technique, the topological variations can be controlled easily.

Active contour can be represented as given in Eq. (1), where $x(S)$ and $y(S)$ are x, y coordinates of the contour and normalized index of points of control is denoted by S.

$$\bar{V}(S) = (\vec{x}(S), \vec{y}(S)) \tag{1}$$

The energy function that defines active contours is comprised of two mechanisms, the external energy, and the internal energy. Internal forces create the curve compact and restrain its deflections that are acuminous. External forces move towards the curve through the borders of the object.

The internal energy of a bending energy and an elastic energy can be represented as given in Eq. (2), where α is an adjustable constant, which denotes continuity, whereas, β is an adjustable constant, which represents curving of contours.

$$e_{\text{int}} = e_{elastic} + e_{bend} = \alpha(S)\left|\frac{dV}{dS}\right|^2 + \beta(S)\left|\frac{d^2V}{dS^2}\right|^2 \tag{2}$$

The bending energies and elastic energies are addressed as given in Eq. (3) and Eq. (4) respectively.

$$e_{bend} = \int_S \beta\left(\vec{V}(S-1) - \vec{V}(S) + \vec{V}(S+1)\right)^2 dS \tag{3}$$

$$e_{elastic} = \int_S \alpha\left(\vec{V}(S) - \vec{V}(S-1)\right)^2 dS \tag{4}$$

The minimized energy function can be represented as given in Eq. (5), where internal energy of the curve is indicated by e_{int}, the picture's energy is denoted by e_{image} and the externals present externally are referred by e_{con}.

$$e^*_{snake} = \int_0^1 e_{snake}(V(S))dS = \int_0^1 \left\{e_{\text{int}}(V(S)) + e_{image}(V(S)) + e_{con}(V(S))\right\}dS \tag{5}$$

Thus the active contour image is obtained which is represented by $A(x, y)$.

Graphcut model

Graph cuts [29] can be applied to solve a large diversity of low-level computer vision issues powerfully like, image segmentation, the stereo correspondence problem, image smoothing and many other computer vision crises, which can be computed regarding the energy minimization. Numerous energy minimization issues can be solved by finding a solution to the maximum flow crises in a graph. Although several computer vision techniques include cutting a graph, the term "graph cuts" is adopted particularly to such models that deploy a max-flow/min-cut optimization.

Image segmentation can be considered as pixel labeling crises. The object's label (s-node) is adjusted to 1 whereas, the background (t-node) is adjusted to 0 and this procedure can be attained by reducing the energy-function by means of minimum graph cut. For making the reasonable segmentation, the cut must occur at the border between background and the object. Most probably, at the object border, the energy or cut should be reduced. Let $L = \{l_1, l_2, l_3 \ldots l_p\}$ where p denotes the number of the pixels in the image and $l_i \in \{0,1\}$.

Therefore, the set L is separated into 2 parts, and the pixel labeled with 1 refers to object whereas the other pixels are grouped into background. The energy function can be reduced by the min-cut in the $s-t$ graph as given in Eq. (6), where, $r(L)$ is called regional parameter that includes the regional details into the segmentation and $b(L)$ is said to be the boundary term that integrates the constraint of boundary into segmentation and the comparative significance feature among boundary and regional term is given by δ. When δ is adjusted to 0, it represents that the regional information is disregarded and only the boundary information is considered.

$$G(L)=\delta\, r(L)+b(L) \tag{6}$$

The energy function in the regional parameter is denoted in Eq. (7), where, $r_p(l_p)$ is the penalty for allocating the label l_p to pixel p. The weight of $r_p(l_p)$ can be achieved by distinguishing the of pixel intensity, p with the provided histogram or intensity model of the background and object.

$$r(L)=\sum_{p\in P} r_p(l_p) \tag{7}$$

The weight of the t-links are described as given in Eq. (8)

$$r_p(1)=-\ln \Pr(I_p|'object') \tag{8}$$

$$r_p(0)=-\ln \Pr(I_p|'background') \tag{9}$$

From Eq. (8) and (9), it can be noticed that when $\Pr(I_p|'background')$ is smaller than $\Pr(I_p|'object')$, $r_p(0)$ will be larger than $r_p(1)$. This represents that when the pixel is more probable to be the object, the grouping of penalty for that pixel into object must be lesser that can minimize the energy in Eq. (6). Therefore, when the entire pixels have been partitioned accurately into two subsets, the regional parameter would be reduced. In Eq. (6), $b(L)$ is the border term that is referred as given in Eq. (10), where p,q are neighboring pixels and $\delta(l_p,l_q)$ is denoted as shown in Eq. (11).

$$b(L)=\sum_{\{p,q\}\in N} b_{<p,q>}.\delta(l_p,l_q) \tag{10}$$

$$\delta(l_p,l_q)=\begin{cases}1 & if\ l_p=l_q\\ 0 & if\ l_p\neq l_q\end{cases} \tag{11}$$

For the regional constriction, it can be interpreted as allocating labels, l_p, l_q to pixels that are placed closer. When the neighboring pixels have the similar labels, the penalty is 0, i.e., the regional term will be able to add only the penalty at the border that is segmented. For the parameter, $b_{<p,q>}$, it is considered as a nonincreasing function of l_p-l_q which is given by Eq. (12), where σ can be observed as camera noise. When the two neighboring pixel's intensity is almost same, there will be a very high penalty or else; it will be low.

$$b_{<p,q>}\alpha \exp\left(\frac{-(l_p-l_q)^2}{2\sigma^2}\right) \tag{12}$$

In Boykov and Jolly's technique, the weight of the $s-t$ graph is represented as shown in Eq. (13), which can also be explained as that, in the $s-t$ graph, when the pixel intensity is considered to be the object, the weight between this pixel and s-node will be greater than that between t-node and pixel which defines that the cut is most probably occurred at the edge with smaller weight.

$$Weight=\begin{cases}b_{<p,q>} & \{p,q\}\in Neighbouring\ pixel\\ \alpha\cdot r_p(0) & for\ edge(p,s)\\ \alpha\cdot r_p(1) & for\ edge(p,t)\end{cases} \tag{13}$$

Thus the resulting partitioned images from graph cut technique are indicated as $B(x,y)$ and $C(x,y)$.

Mutual segmentation using Graph cut plus Active contour

After partitioning the image, $I(x,y)$ by using Graph cut technique, the outcome of Graph cut image, $B(x,y)$ and $C(x,y)$ is compared with the active contour image $A(x,y)$. The mutual information of images, $B(x,y)$ and $A(x,y)$ are taken, which is indicated by $D(x,y)$. Similarly, mutual information of $C(x,y)$ and $A(x,y)$ are noted and is represented as $E(x,y)$.

Grouping low and high-intensity pixels

The images $D(x,y)$ and $E(x,y)$ are further partitioned into low and high-intensity images using FEM method. As the objective is to divide pixels into two fuzzy sets, only the W-function and Z-function are needed as the membership functions to construct Fuzzy 2- partition entropy [26] [30]. The fuzzy 2-partition entropy is described as given in Eq. (14).

$$H=-F_d\log(F_d)-F_b\log(F_b) \tag{14}$$

As the probability of the bright set E_b can be considered as $F_b=1-F_d$, the fuzzy entropy can be modified as given in Eq. (15) and also the value of F_d can be rewritten as given in Eq. (16), where u,v,w are the parameters describing the shape of the W membership functions that satisfy the constraint $0\le u<v<w\le 255$. The value of H in Eq. (15) represents both H_1 and H_2, where $H_1=H(D(x,y))$ and $H_2=H(E(x,y))$.

$$H=-F_d\log(F_d)-(1-F_d)\log(1-F_d) \tag{15}$$

$$F_d=\frac{1}{(w-u)(w-v)}\sum_{k=v+1}^{w}(k-w)^2h(k)\ - \frac{1}{(w-u)(v-u)}\sum_{k=u+1}^{v}(k-u)^2h(k)+\sum_{k=0}^{v}h(k) \tag{16}$$

To carry out the exhaustive exploration, the fuzzy entropy H values under all suitable u, v, w settings are calculated by means of pre-stored iterative values of F_d . The optimal set of factors that maximize H is chosen. Thus the images $D(x, y)$ and $E(x, y)$ are split into low-intensity images $D_1(x, y)$ and $E_1(x, y)$ and high-intensity images of $D_2(x, y)$ and $E_2(x, y)$ respectively.

EXPERIMENTAL SET-UP

The proposed AGFES-based image segmentation model was implemented in MATLAB using Weizmann database is used which is downloaded from http://www.wisdom.weizmann.ac.il/~vision/Seg_Evaluation_DB/ with seven sets of images. That data set includes animals, birds, nature, objects, transportation, and tree. In each set, a particular number of images were available, i.e., for animals, 12 images were considered, for birds, 15 images were considered, for objects, 26 images were considered, for transportation, 9 images were considered, for tree, 10 images were considered. The implemented method is compared with GS [29], SLGS [30], FES [31] and GFES [32] by analyzing the performance measures [33][34][35] like accuracy, sensitivity, specificity, precision, FPR, FNR, NPV, FDR, F1-score, and MCC are analyzed. The results of simulation show the enhanced performance of the implemented AGFES method. Fig 2 gives the sample images for each dataset and its corresponding segmentation outputs.

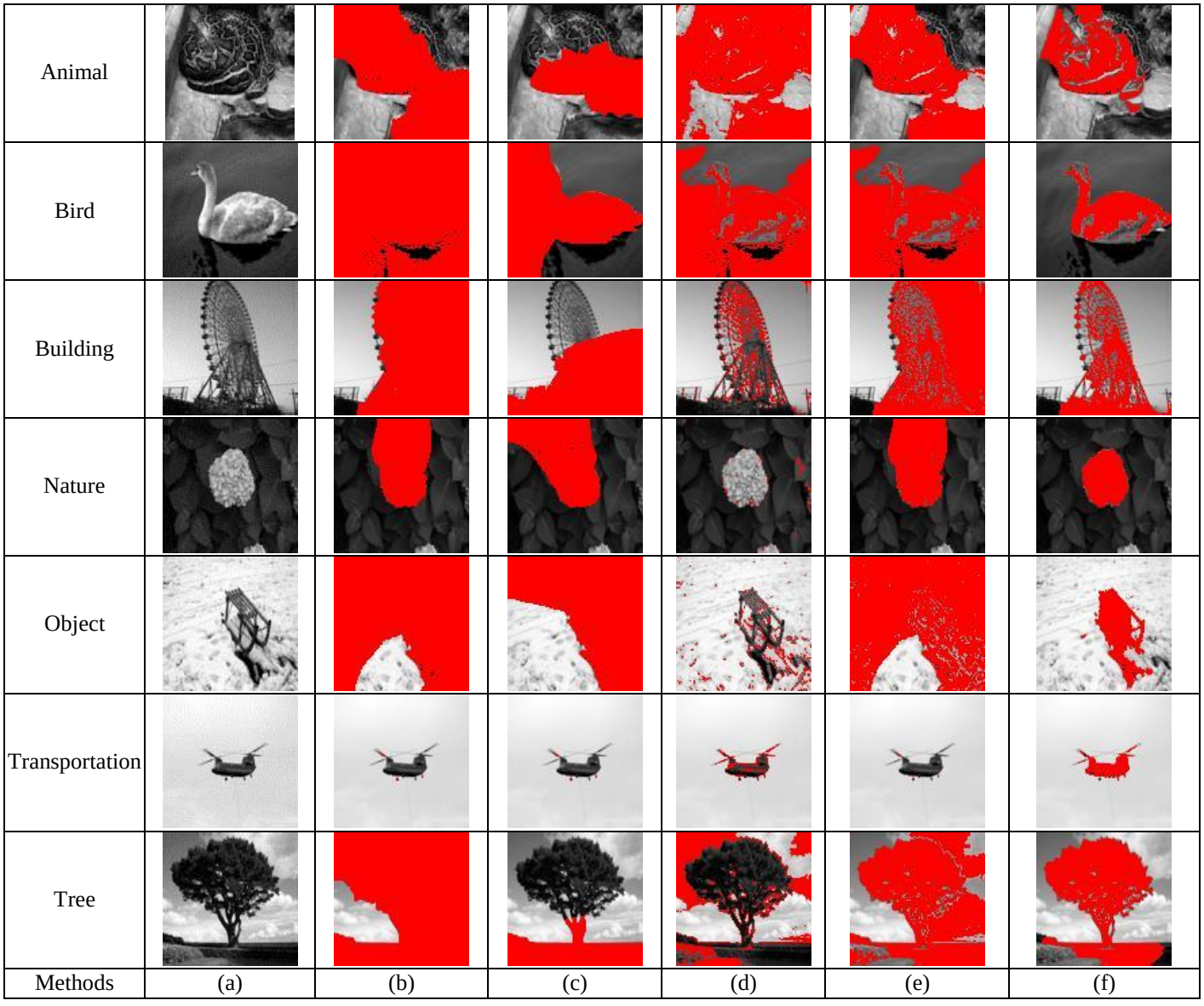

Figure 2: Sample images for each dataset and its corresponding segmented output for different methods like (a) Original image, (b) GS (c)SLGS (d) FES (e) GFES (f)AGFES

RESULTS AND DISCUSSIONS

Performance analysis

The performance analysis of the proposed AGFES-based segmentation over the conventional methods for test case 1 is given by Table II. From Table II, for test case 1, the implemented method in terms of accuracy is 33.9% better than GS, 42.5% better than SLGS, 30.8% better than FES and 19.7% better than GFES techniques. Similarly, the implemented method regarding sensitivity is 41.2% superior to GS, 1.48% superior to SLGS, 60.6% superior to FES and 7.8% superior to GFES techniques. On considering specificity, the proposed method is 47.5% better than GS, 50.7% better than SLGS, 49.6% better than FES and 25.6% better than GFES techniques. Moreover, the proposed AGFES method in terms of precision is 57.6% superior to GS, 67.5% superior to SLGS, 53.8% superior to FES and 48.8% superior to GFES techniques. On considering F-score, the proposed method is 23.5% better than GS, 42.8% better than SLGS, 31.9% better than FES and 22.6% better than GFES techniques.

Similarly, from Table III, for test case 2, the implemented method in terms of accuracy is 33.7% better than GS, 42.8% better than SLGS, 48% better than FES and 29.8% better than GFES techniques. Similarly, the implemented method regarding sensitivity is 75.8% superior to GS, 0.6% superior to SLGS, 87% superior to FES and 20% superior to GFES techniques. On considering specificity, the proposed method is 52.8% better than GS, 50.7% better than SLGS, 71.6% better than FES and 38.1% better than GFES techniques. Moreover, the proposed method in terms of precision is 56.1% superior to GS, 69% superior to SLGS, 62.5% superior to FES and 23.8% superior to GFES techniques Also the implemented method in terms of NPV is 52% superior to GS, 50.7% superior to SLGS, 70.9% superior to FES and 38.1% superior to GFES techniques.

Moreover, from Table IV, for test case 3, the proposed method on considering accuracy is 27.9% better than GS, 26.5% better than SLGS, 42.7% better than FES and 20.6% better than GFES techniques. Similarly, the implemented method in terms of sensitivity is 10.23% superior to GS, 44.3% superior to SLGS, 94.2% superior to FES and 21.2% superior to GFES techniques. On considering specificity, the proposed method is 32.4% better than GS, 37.5% better than SLGS, 64.5% better than FES and 20.9% better than GFES techniques. Moreover, the proposed method regarding precision is 37.8% superior to GS, 27.3% superior to SLGS, 30.4% superior to FES and 42.3% superior to GFES techniques.

Also, from Table V, for test case 4, the proposed method regarding accuracy is 41.3% better than GS, 34.2% better than SLGS, 51.3% better than FES and 34.3% better than GFES techniques. Similarly, the implemented method in terms of sensitivity is 2.54% superior to GS, 26.9% superior to SLGS, 87.9% superior to FES and 24.3% superior to GFES techniques. On considering specificity, the proposed method is 48.7% better than GS, 43% better than SLGS, 72.6% better than FES and 35% better than GFES techniques. Moreover, the proposed method regarding precision is 62.1% superior to GS, 51.1% superior to SLGS, 52% superior to FES and 63.9% superior to GFES techniques. Similarly, the implemented method regarding FNR is 62% superior to FES technique, but the performance of GS, SLGS, and GFES are more when compared with the proposed technique. However, the accuracy is more in the proposed method than FNR, and hence the performance of FNR can be considered negligible.

Moreover, from Table VI, for test case 5, the proposed method on considering accuracy is 36.7% better than GS, 37.9% better than SLGS, 50.6% better than FES and 30.3% better than GFES techniques. Similarly, the implemented method regarding sensitivity is 21.3% superior to GS, 15.1% superior to SLGS, 60.4% superior to FES and 1.27% superior to GFES techniques. On considering specificity, the proposed method is 47.8% better than GS, 48.7% better than SLGS, 72.1% better than FES and 35.3% better than GFES techniques. Moreover, the proposed method regarding precision is 55% superior to GS, 58.3% superior to SLGS, 56.7% superior to FES and 55% superior to GFES techniques.

Similarly, from Table VII, for test case 6, the proposed method on considering accuracy is 39.6% better than GS, 40.8% better than SLGS, 59.3% better than FES and 33.4% better than GFES techniques. Similarly, the implemented method regarding sensitivity is 10.8% superior to GS, 0.98% superior to SLGS, 54.4% superior to FES and 8.9% superior to GFES techniques. On considering specificity, the proposed method is 47.5% better than GS, 47.4% better than SLGS, 79.1% better than FES and 37.4% better than GFES techniques. Moreover, the proposed method regarding precision is 60% superior to GS, 62.5% superior to SLGS, 63.3% superior to FES and 60.8% superior to GFES techniques.

Also, from Table VIII, for test case 7, the proposed method in terms of accuracy is 33.1% better than GS, 39.5% better than SLGS, 48.5% better than FES and 27.1% better than GFES techniques. Similarly, the implemented method in terms of sensitivity is 14.6% superior to GS, 1.62% superior to SLGS, 68.7% superior to FES and 5.5% superior to GFES techniques. On considering specificity, the proposed method is 43.1% better than GS, 48.7% better than SLGS, 74% better than FES and 32% better than GFES techniques. Moreover, the proposed method regarding precision is 53.8% superior to GS, 59.8% superior to SLGS, 56.6% superior to FES and 52.4% superior to GFES techniques. Similarly, the proposed method in terms of MCC is 87% better than GS, 90% better than SLGS and 95% better than FES and 88% better than GFES techniques. Moreover, the proposed method regarding FPR is 81.8% superior to GS, 81.81% superior to SLGS, 88% superior to FES and 78% superior to GFES techniques. Further, the proposed method in terms of FDR is 57% better

than GS, 60% better than SLGS, 58% better than FES and 56% better than GFES techniques. Thus the performance of the proposed AGFES based image segmentation system in terms of certain measures is verified.

TABLE II.Evaluation of type I and type II measures on proposed and conventional image segmentation methods for test case 1

Measures	GS[28]	SLGS[29]	FES[30]	GFES[31]	AGFES
Accuracy	0.548883	0.475375	0.566817	0.656817	0.817842
Sensitivity	0.668415	0.48369	0.767186	0.517341	0.472994
Specificity	0.501749	0.472096	0.487805	0.711816	0.953825
Precision	0.345977	0.265409	0.371322	0.414481	0.801558
FPR	0.498251	0.527904	0.512195	0.288184	0.046175
FNR	0.331585	0.51631	0.232814	0.482659	0.527006
NPV	0.501749	0.472096	0.487805	0.711816	0.953825
FDR	0.654023	0.734591	0.628678	0.585519	0.198442
F-score	0.455951	0.342747	0.500432	0.460234	0.594926
MCC	0.153935	-0.03984	0.233015	0.215953	0.515523

TABLE III. Evaluation of type I and type II measures on proposed and conventional image segmentation methods for test case 2

Measures	GS[28]	SLGS[29]	FES[30]	GFES[31]	AGFES
Accuracy	0.51155	0.447083	0.400208	0.546667	0.769883
Sensitivity	0.639907	0.384268	0.674968	0.439291	0.358229
Specificity	0.454284	0.475108	0.277624	0.594572	0.953542
Precision	0.343468	0.246206	0.294219	0.325879	0.774785
FPR	0.545716	0.524892	0.722376	0.405428	0.046458
FNR	0.360093	0.615732	0.325032	0.560709	0.641771
NPV	0.454284	0.475108	0.277624	0.594572	0.953542
FDR	0.656532	0.753794	0.705781	0.674121	0.225215
F-score	0.447006	0.30012	0.409804	0.37418	0.489933
MCC	0.087999	-0.12999	-0.04815	0.031734	0.411774

TABLE IV. Evaluation of type I and type II measures on proposed and conventional image segmentation methods for test case 3

Measures	GS[28]	SLGS[29]	FES[30]	GFES[31]	AGFES
Accuracy	0.498543	0.510138	0.399176	0.542867	0.6805
Sensitivity	0.427038	0.556125	0.7466	0.304113	0.380988
Specificity	0.523325	0.4942	0.278767	0.625613	0.784304
Precision	0.236925	0.275918	0.264038	0.219678	0.379716
FPR	0.476675	0.5058	0.721233	0.374387	0.215696
FNR	0.572962	0.443875	0.2534	0.695887	0.619012
NPV	0.523325	0.4942	0.278767	0.625613	0.784304
FDR	0.763075	0.724082	0.735962	0.780322	0.620284
F-score	0.304764	0.368839	0.390112	0.25509	0.380351
MCC	-0.04351	0.044034	0.024916	-0.06415	0.165111

TABLE V. Evaluation of type I and type II measures on proposed and conventional image segmentation methods for test case 4

Measures	GS[28]	SLGS[29]	FES[30]	GFES[31]	AGFES
Accuracy	0.446886	0.50701	0.374348	0.508762	0.760776
Sensitivity	0.428395	0.521735	0.772973	0.313872	0.409593
Specificity	0.453049	0.502102	0.241486	0.573719	0.877825
Precision	0.207012	0.258851	0.253538	0.197051	0.527721
FPR	0.546951	0.497898	0.758514	0.426281	0.122175
FNR	0.571605	0.478265	0.227027	0.686128	0.590407
NPV	0.453049	0.502102	0.241486	0.573719	0.877825
FDR	0.792988	0.741149	0.746462	0.802949	0.472279
F-score	0.279138	0.346026	0.381833	0.242106	0.461213
MCC	-0.10273	0.020643	0.014704	-0.09943	0.314714

TABLE VI. Evaluation of type I and type II measures on proposed and conventional image segmentation methods for test case 5

Measures	GS[28]	SLGS[29]	FES[30]	GFES[31]	AGFES
Accuracy	0.506415	0.490488	0.39495	0.557842	0.789985
Sensitivity	0.596347	0.560997	0.781393	0.480195	0.486185
Specificity	0.474812	0.46571	0.259145	0.585129	0.896746
Precision	0.285222	0.269533	0.27042	0.289144	0.623312
FPR	0.525188	0.53429	0.740855	0.414871	0.103254
FNR	0.403653	0.439003	0.218607	0.519805	0.513815
NPV	0.474812	0.46571	0.259145	0.585129	0.896746
FDR	0.714778	0.730467	0.72958	0.710856	0.376688
F-score	0.385883	0.364122	0.40179	0.360948	0.546275
MCC	0.062668	0.023511	0.041144	0.05785	0.417737

TABLE VII. Evaluation of Type I And Type II Measures On Proposed And Conventional Image Segmentation Methods For Test Case 6

Measures	GS[28]	SLGS[29]	FES[30]	GFES[31]	AGFES
Accuracy	0.499027	0.487738	0.334531	0.543365	0.811854
Sensitivity	0.566468	0.516515	0.78154	0.462056	0.505042
Specificity	0.477649	0.478617	0.192837	0.569139	0.909108
Precision	0.255816	0.238978	0.234842	0.253694	0.637853
FPR	0.522351	0.521383	0.807163	0.430861	0.090892
FNR	0.433532	0.483485	0.21846	0.537944	0.494958
NPV	0.477649	0.478617	0.192837	0.569139	0.909108
FDR	0.744184	0.761022	0.765158	0.746306	0.362147
F-score	0.352462	0.326769	0.361161	0.327547	0.563731
MCC	0.037803	-0.00417	-0.02744	0.026877	0.450791

TABLE VIII. EVALUATION OF TYPE I AND TYPE II MEASURES ON PROPOSED AND CONVENTIONAL IMAGE SEGMENTATION METHODS FOR TEST CASE 7

Measures	GS[28]	SLGS[29]	FES[30]	GFES[31]	AGFES
Accuracy	0.526612	0.473927	0.407542	0.566677	0.77735
Sensitivity	0.534782	0.474949	0.786087	0.437532	0.462477
Specificity	0.522963	0.47347	0.238518	0.624341	0.917944
Precision	0.333582	0.287124	0.315508	0.342128	0.715633
FPR	0.477037	0.52653	0.761482	0.375659	0.082056
FNR	0.465218	0.525051	0.213913	0.562468	0.537523
NPV	0.522963	0.47347	0.238518	0.624341	0.917944
FDR	0.666418	0.712876	0.684492	0.657872	0.284367
F-score	0.410873	0.35789	0.450287	0.383993	0.561855
MCC	0.053354	-0.04767	0.026972	0.058475	0.439763

STATISTICAL ANALYSIS

The statistical analysis for the implemented AGFES-based image segmentation is given by Fig. 3. From Fig. 3(a), the accuracy of proposed AGFES method in terms of best performance is 32.9% better than GS, 39% better than SLGS, 29.2% better than FES and 20.7% better than GFES techniques. Similarly, from Fig. 3(b), the sensitivity of the implemented method regarding best performance is 14.3% superior to GS, 11.4% superior to SLGS, 97.1% superior to FES and 14.2% superior to GFES techniques. On considering the mean in Fig. 3(c), the specificity of the proposed method is 44.4% better than GS, 45.6% better than SLGS, 66.7% better than FES and 33.3% better than GFES techniques. Moreover, from Fig. 3(d), the precision of the proposed method regarding mean is 53.8% superior to GS, 56.9% superior to SLGS, 55.3% superior to FES and 55.3% superior to GFES techniques. Similarly, from Fig. 3(e), the FPR of the implemented method in terms of median is 90% superior to GS, 90% superior to SLGS, 92.8% superior to FES and 70% superior to GFES techniques. On considering the performance of mean in Fig. 3(f), the FNR of proposed method is 18.1% better than GS, 10% better than SLGS, 54.5% better than FES and 10% better than GFES techniques. Moreover, from Fig. 3 (g), NPV of the proposed method in terms of median is 55.5% superior to GS, 55.5% superior to SLGS, 66.6% superior to FES and 35.6% superior to GFES techniques. Also, from Fig. 3(h), FDR of the proposed method in terms of standard deviation is 75% better than GS, 90% better than SLGS, 85% better than FES and 50% better than GFES techniques. Moreover, from Fig. 3 (i), F-score of the proposed method in terms of mean is 25% superior to GS, 50% superior to SLGS, 16.6% superior to FES and 25% superior to GFES techniques. Also from Fig. 3(j), MCC of the proposed AGFES method in terms of best performance is 62% better than GS, 90% better than SLGS, 50% better than FES and 60% better than GFES techniques Thus the capability of the implemented AGFES for image segmentation is validated.

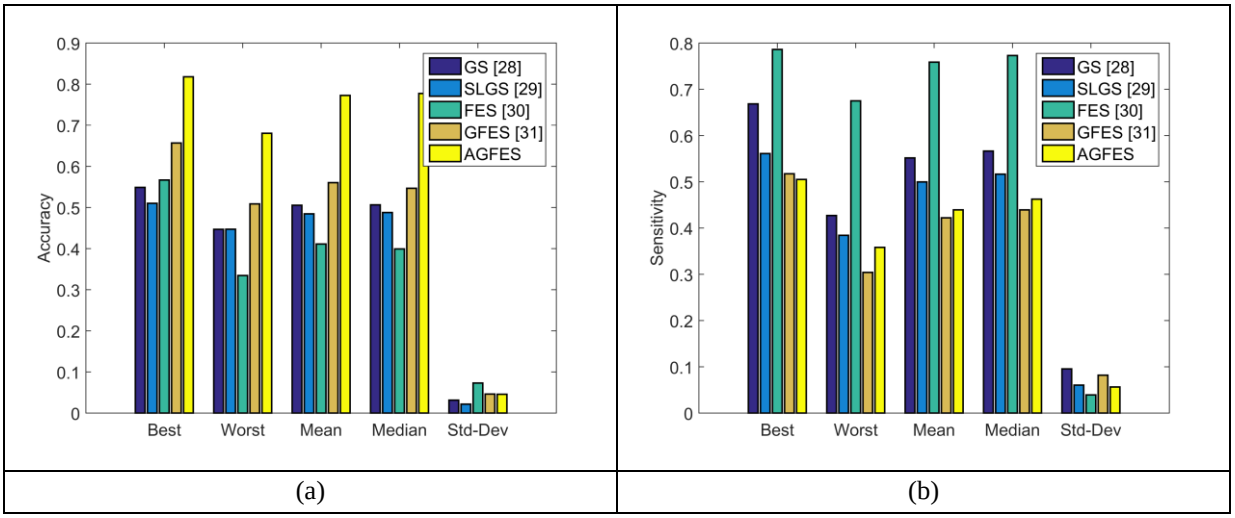

(a) (b)

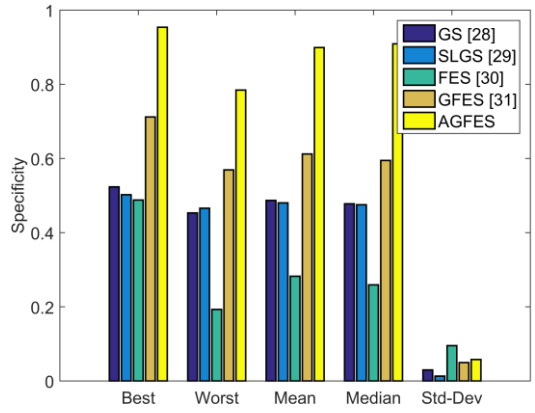
Specificity
GS [28]
SLGS [29]
FES [30]
GFES [31]
AGFES
Best
Worst
Mean
Median
Std-Dev

(c)

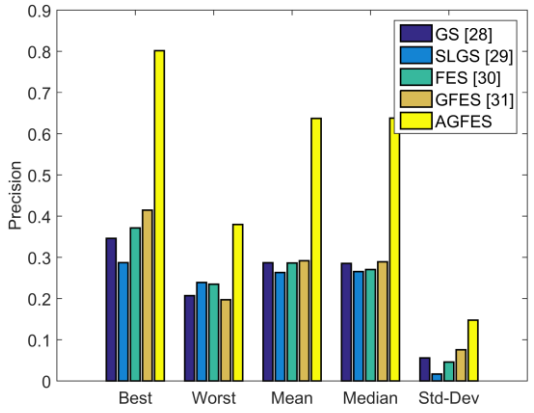
Precision
GS [28]
SLGS [29]
FES [30]
GFES [31]
AGFES
Best
Worst
Mean
Median
Std-Dev

(d)

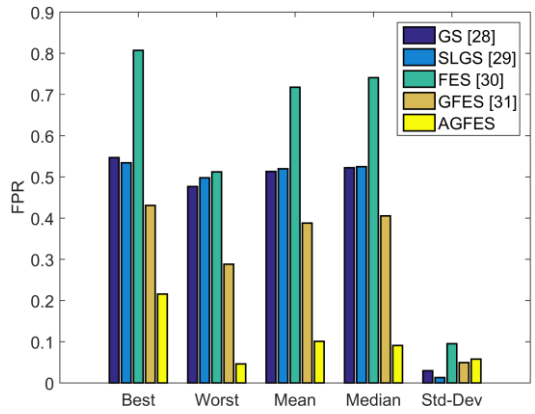
FPR
GS [28]
SLGS [29]
FES [30]
GFES [31]
AGFES
Best
Worst
Mean
Median
Std-Dev

(e)

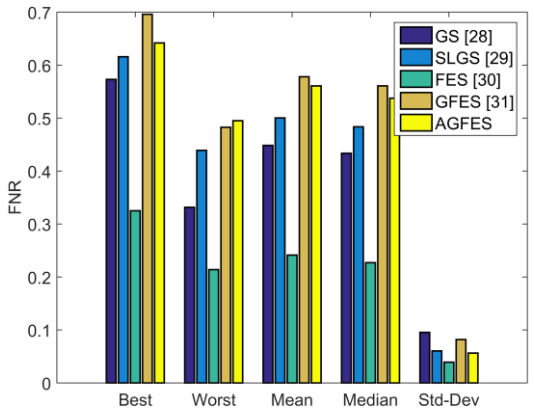
FNR
GS [28]
SLGS [29]
FES [30]
GFES [31]
AGFES
Best
Worst
Mean
Median
Std-Dev

(f)

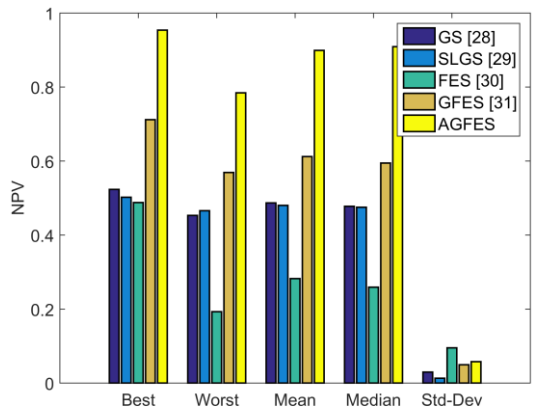
NPV
GS [28]
SLGS [29]
FES [30]
GFES [31]
AGFES
Best
Worst
Mean
Median
Std-Dev

(g)

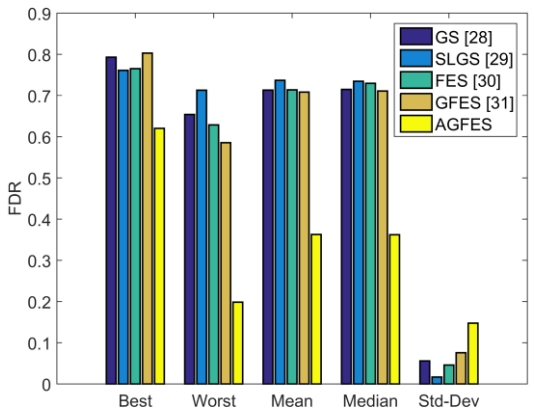
FDR
GS [28]
SLGS [29]
FES [30]
GFES [31]
AGFES
Best
Worst
Mean
Median
Std-Dev

(h)

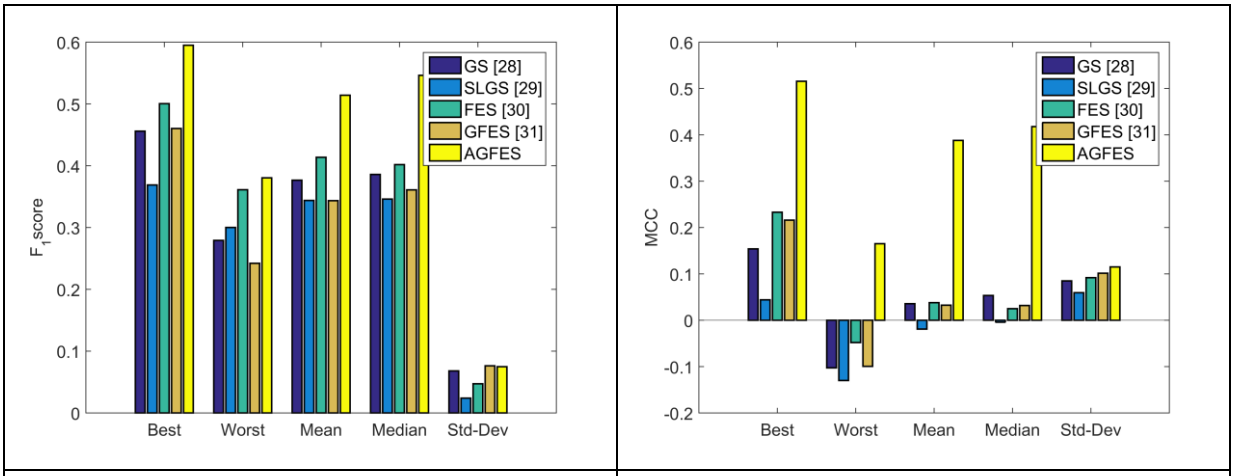

Figure 3: Statistical analysis of proposed and conventional image segmentation techniques (a) Accuracy (b) Sensitivity (c) Speificity (d) Precision (e) FPR (f) FNR (g) NPV (h) FDR (i) F1-Score (j) MCC

CONCLUSION

This paper has presented AGFES technique which has solved the problem in segmenting the images accurately by using traditional active contour models that are solved by a novel active contour model based on modified symmetric cross entropy. The process was further followed by a Graph cut technique and a Fuzzy entropy based optimization was applied that had brought out the enhanced low-intensity and high-intensity images. Moreover, the extensive experiments were performed on a large number of images, and the results have demonstrated that the proposed method in terms of accuracy was 39.6% better than GS, 40.8% better than SLGS, 59.3% better than FES and 33.4% better than GFES techniques. Similarly, the implemented method in terms of sensitivity was 10.8% superior to GS, 0.98% superior to SLGS, 54.4% superior to FES and 8.9% superior to GFES techniques. On considering specificity, the proposed method was 47.5% better than GS, 47.4% better than SLGS, 79.1% better than FES and 37.4% better than GFES techniques. Moreover, the proposed method in terms of precision was 60% superior to GS, 62.5% superior to SLGS, 63.3% superior to FES and 60.8% superior to GFES techniques. Thus the capability of the implemented AGFES technique for segmenting the images was demonstrated successfully.

This paper has achieved encouraging image segmentation result using FEM with Non-Linear Programming. In future, more advanced optimization algorithm can be used for maximizing the entropy in FEM technique to improve the segmentation accuracy.

REFERENCES

[1] M. Jogendra Kumar, Dr. GVS Raj Kumar, R. Vijay Kumar Reddy, "Review on Image Segmentation Techniques",International Journal of Scientific Research Engineering & Technology, vol. 3, no. 6, pp. 2278 – 0882, September 2014.

[2] Yiping Duan, Fang Liu, Licheng Jiao, Peng Zhao, Lu Zhang, " SAR Image segmentation based on convolution-wavelet neural network and Markov random field", Pattern Recognition, vol. 64, pp. 255-267, April 2017.

[3] M. Guijarro, I. Riomoros, G. Pajares, P. Zitinski, " Discrete wavelets transform for improving greenness image segmentation in agricultural images", Computers and Electronics in Agriculture, vol.118, pp 396-407, October 2015.

[4] Jianning Chi, Mark Eramian, "Enhancing textural differences using wavelet-based texture characteristics morphological component analysis: A pre-processing method for improving image segmentation", Computer Vision and Image Understanding, vol.158, pp. 49-61, May 2017.

[5] Siu Kai Choy, Shu Yan Lam, Kwok Wai Yu, Wing Yan Lee, King Tai Leung, "Fuzzy model-based clustering and its application in image segmentation", Pattern Recognition, vol. 68, pp.141-157, August 2017.

[6] Zhang Yong, Yuan Jiazheng, Liu Hongzhe, Li Qing, "Grab-Cut image segmentation algorithm based on structure tensor", The Journal of China Universities of Posts and Telecommunications, vol. 24, no. 2, pp. 38-47, April 2017.

[7] Yafeng Li, Xiangchu Feng, "A multi-scale image segmentation method", Pattern Recognition, vol.52, pp. 332-345, April 2016.

[8] Yongsheng Pan, Yong Xia, Tao Zhou, Michael Fulham, "Cell image segmentation using bacterial foraging optimization", Applied Soft Computing, vol. 58, pp.770-782, September 2017.

[9] Weiwei Wang, Cuiling Wu, "Image segmentation by correlation adaptive weighted regression", Neuro computing , 29 June 2017.

[10] Jerrod Ankenman, William Leeb, "Mixed Hölder matrix discovery via wavelet shrinkage and Calderón–Zygmund decompositions", Applied and Computational Harmonic Analysis, , 25 January 2017.

[11] Tao Bing; Haihui Wang; Shangmei Zhao,"Correspondence between nonlinear diffusion and M-band wavelet shrinkage", IEEE Conference Publications, 2nd IEEE International Conference on Computer and Communications (ICCC), pp. 1980 - 1984, 2016.

[12] Behzad Kamgar-Parsi; Behrooz Kamgar-Parsi; Kian Kamgar-Parsi,"Notes on image processing with partial differential equations", IEEE Conference Publications, pp. 1737 – 1741, 2015.

[13] Iasonas Kokkinos; Petros Maragos, "Synergy between Object Recognition and Image Segmentation Using the Expectation-Maximization Algorithm", IEEE Journals & Magazines, vol.31, no.08, pp.1486 - 1501, 2009.

[14] Yousun Kang; Koichiro Yamaguchi; Takashi Naito; Yoshiki Ninomiya,"Multiband Image Segmentation and Object Recognition for Understanding Road Scenes", IEEE Journals & Magazines, vol.12, no.04, pp.1423 - 1433, 2011

[15] Fuzhuan Wu, Bingxin Wu,"Design and Realization of Fuzzy Control System for Textile Mill's Air-Conditioning Based on MSP430", IEEE Conference Publications, pp.1 - 4, 2010.

[16] Jiangyang Zhang; Rongjie Lai; C. -C. Jay Kuo ,"Adaptive Directional Total-Variation Model for Latent Fingerprint Segmentation", IEEE Journals & Magazines, vol.08, no.08, pp.1261 – 1273, 2013.

[17] Snehashis Roy; Qing He; Elizabeth Sweeney; Aaron Carass; Daniel S. Reich; Jerry L. Prince; Dzung L. Pham, "Subject-Specific Sparse Dictionary Learning for Atlas-Based Brain MRI Segmentation", IEEE Journals & Magazines, vol. 19, no.05, pp. 1598 - 1609, 2015.

[18] Gang Zheng; Yuanlu Li; Huinan Wang, "A New Multi-phase Level Set Framework for 3D Medical Image Segmentation Based on TPBG", IEEE Conference Publications, pp.3394 - 3397, 2005.

[19] Zhuowen Tu; Song-Chun Zhu, "Image segmentation by data-driven Markov chain Monte Carlo", IEEE Journals & Magazines , vol.24, no.05, pp.657 - 673, 2002.

[20] Iason Papaioannou, Wolfgang Betz, Kilian Zwirglmaier, Daniel Straub,"MCMC algorithms for Subset Simulation", Probabilistic Engineering Mechanics, vol.41, pp.89-103, July 2015.

[21] Jianbo Shi; J. Malik,"Normalized cuts and image segmentation", IEEE Conference Publications, pp. 731 - 737, 1997.

[22] Shifeng Chen; Liangliang Cao; Yueming Wang; Jianzhuang Liu; Xiaoou Tang, "Image Segmentation by MAP-ML Estimations", IEEE Journals & Magazines, vol.19, no.09, pp. 2254 - 2264, 2010.

[23] A. Polesel; G. Ramponi; V. J. Mathews,"Image enhancement via adaptive unsharp masking", IEEE Journals & Magazines, vol. 9, no.03, pp.505 - 510, 2000.

[24] Changjae Oh, Bumsub Ham, Kwanghoon Sohn, "Robust interactive image segmentation using structure-aware labelling", Expert Systems with Applications, vol. 79, pp. 90-100, 15 August 2017.

[25] Dachun Zhang; Gang Liu; Hongbin Li; Deqiang Chu; Yuebin Kang, "Block Adaptive Bayesian Wavelet Shrinkage for 2D Signal De-noising", IEEE Conference Publications, Vol.3, pp.302 - 306, 2008.

[26] Kyumok Kim; Seung-Won Jung," Interactive Image Segmentation using Semi-transparent Wearable Glasses", IEEE Transactions on Multimedia, Vol. PP, no. 99, pp. 1 – 1, 2017.

[27] A. Mousa, M. El-Shorbagy, W. Abd-El-Wahed, "Local search based hybrid particle swarm optimization algorithm for multiobjective optimization", Swarm and Evolutionary Computation, vol. 3, pp. 1-14, 2012.

[28] Lei Wang, Yan Chang, Hui Wang, Zhenzhou Wu, Xiaodong Yang, " An active contour model based on local fitted images for image segmentation",Information Sciences, vol. 418–419, pp. 61-73, December 2017.

[29] F. Yi and I. Moon, "Image segmentation: A survey of graph-cut methods," 2012 International Conference on Systems and Informatics (ICSAI2012), Yantai, pp. 1936-1941, 2012.

[30] Dayong Ren, Zhenhong Jia, Jie Yang and Nikola K.

Kasabov, "A Practical GrabCut Color Image Segmentation Based on Bayes Classification and Simple Linear Iterative Clustering", IEEE Access, vol.5, pp.18480 - 18487, September 2017.

[31] Shibai Yin , Yiming Qian , Minglun Gong, "Unsupervised Hierarchical Image Segmentation through Fuzzy Entropy Maximization", Pattern Recognition, vol.68, pp.245-259, August 2017.

[32] ShibaiYin, XiangmoZhao, WeixingWang and MinglunGong, "Efficient multilevel image segmentation through fuzzy entropy maximization and graph cut optimization", Pattern Recognition, vol.47, no.9, pp.2894-2907, September 2014.

[33] Powers, David M.W. (2011), "Evaluation: From Precision, Recall and F-Measure to ROC, Informedness, Markedness and Correlation", Journal of Machine Learning Technologies, Vol.2(1),pp.37-63

[34] G.V.S. Rajkumar, Srinivasa Rao K. and Srinivasa Rao P.(2011), "Image Segmentation Method Based On Finite Doubly Truncated Bivariate Gaussian Mixture Model with Hierarchical Clustering", IJCSI International Journal of Computer Science Issues, Vol. 8, Issue 4, No 2, pp.151-159.

[35] K.Naveen Kumar; K.Srinivasa Rao; Y.Srinivas And Ch.Satyanarayana, "Studies on Improving Texture Segmentation Performance using Generalized Gaussian Mixture Model Integrating DCT And LBP", Journal of Theoretical and Applied Information Technology , vol.92(2), pp. 200-207, October, 2016

[36] R.A.Waltz, J.L. Morales, J. Nocedal and• D. Orban, " An interior algorithm for nonlinear optimization that combines line search and trust region steps", Digital Object Identifier, vol. 107, pp. 391–408, 2006.